14 (2022) 100141

Contents lists available at ScienceDirect

International Journal of Thermofluids

journal homepage: www.sciencedirect.com/journal/international-journal-of-thermofluids

Three-dimensional high-resolution image inversion and pore level CFD characterisation of effective thermal conductivity of replicated microcellular structures

A.J. Otaru [a,*], M. Abdulkadir [a], A.S. Kovo [a], M.R. Corfield [b], N. Tanko [c], O.A. Odey [d], A. Kenfack [e], U.O. Aroke [f]

[a] Department of Chemical Engineering, Federal University of Technology, P.M.B. 065, Gidan-Kwanu Campus, Minna, Nigeria
[b] Department of Electrical & Electronic Engineering, The University of Nottingham, Nottingham, NG7 2RD, United Kingdom
[c] Department of Petroleum and Natural Gas Engineering, Baze University, Plot 686, Cadastral Zone C 00, Jabi Airport Road Bypass, F.C.T. Abuja, Nigeria
[d] Department of Chemical Engineering, University of Calabar, P.M.B. 1115, Etagbor Road, Calabar, Nigeria
[e] African University of Science and Technology, Km 10 Airport Road, P.M.B. 681, Galadimawa, F.C.T. Abuja, Nigeria
[f] Department of Chemical Engineering, Abubakar Tafawa Balewa University, P.M.B. 0248, Bauchi, Nigeria

ARTICLE INFO

Keywords:
Microcellular metals
Computational fluid dynamics
Effective thermal conductivity

ABSTRACT

Metallic-based microcellular structures are widely used in heat and mass transfer processes owing to their unique combination of high porosity, high surface area, fixed pore morphology and high Young modulus, enabling their suitability as heat pipes in oil and gas processing equipment, biomedical materials for bone repair and bone substitution, solar collectors, fuel cells, impact loading, soundproofing materials and metallurgical processing. Accurate representation of the effective thermal conductivity of these materials is imperative in understanding their heat transfer mechanisms leading to the design and optimisation of system performance. Due to the limited availability of experimental and predictive data on heat transport phenomena across the interstices of low-porosity microcellular structures - numerically simulated data of effective thermal conductivity for conduction heat transfer in metal foam-fluid systems have been compared for structures typified by near-circular pore walls and openings, i.e. "bottleneck-type" structures and foam porosity ranging between 0.65 and 0.78. A three-dimensional high-resolution image inversion and computational fluid dynamics modelling and simulation of conductive heat transfer for both the fluid and solid domains at pore level is used to estimate effective thermal conductivity for these structures. This approach is extended to structurally-adapted metal foam-fluid systems by broadening the pore volume fraction beyond 0.90 – resulting in the quantification of the fluid phase contribution for heat transfer enhancement and the proposition of empirical constants to support models developed by Calmidi & Mahajan [9]. Findings in this work offer strong support to the supposition that geometrical adaptions of microcellular structures can be used to modulate their effective thermal conductivity and that generalised values of empirical constants may be ambiguous to fully describe conduction heat transfer phenomena in microcellular structures. This approach may prove useful in the design of low-porosity metallic components for applications specific to conduction heat transfer.

Introduction

The past twenty years have witnessed a rise in the production and utilisation of metallic-based microcellular structures in the construction of home, laboratory and industrial process equipment, and as supporting material for vibration and emission reduction control. The production costs of these materials have also been reduced as a result of the increased production of metallic components across the globe [1]. Porous metallic structures are typically classified as open-celled or closed-celled foams [2–5]. These materials are distinguished from packed beds by their unique and interconnected pore openings (also known as "windows") and complex ligaments or struts (as shown by Fig. 1a) facilitating their suitability as packing structures in electrolytic [6, 7], aerospace and automobile applications and other heat exchange

* Corresponding author.
E-mail address: otaru.jinadu@futminna.edu.ng (A.J. Otaru).

https://doi.org/10.1016/j.ijft.2022.100141
Received 14 October 2021; Received in revised form 17 February 2022; Accepted 18 February 2022
Available online 19 February 2022

and mass transfer process equipment [6–10]. This, therefore, makes the effective thermal conductivity (k_{eff}) of metal foam-fluid systems important in the design and selection of porous metallic materials for applications specific to heat and mass (energy) transfer.

Unlike packed bed structures, the complex morphological features of porous metals make it difficult to unequivocally define the effects of individual heat transfer mechanisms on the effective thermal conductivity of a metal foam-fluid system. The premise of determining the effective thermal conductivity of metal foam-fluid systems can be traced back to the experimental work conducted on air- and water-saturated high porosity ($0.9 \leq \varepsilon \leq 0.98$) fibrous foams by Calmidi & Mahajan [9]. Their empirical data showed a linear inverse relationship between foam porosity and effective thermal conductivity with no systematic influence of pore density observed. An evaluation of the effective thermal conductivity and flow permeability of fluid saturated aluminium foams was reported in [10]. The effective thermal conductivity was observed to increase with decreasing porosity with no perceptible change observed with variable cell size. Experimental measurements of the effective thermal conductivity of selected solid aluminium alloy 6101-T6 (with porosities: 0.69, 0.78 and 0.80) saturated with air was reported in [11]. These low porosity foams were achieved by compressing highly porous foam characterised by a porosity of 92%. Foam porosity was observed to decrease with increasing level of applied compressive force with the resulting evaluated values of the effective thermal conductivity exhibiting a linear inverse relationship with foam porosity, consistent with the description given in [9, 10]. Sadeghi et al [12]. further investigated the effects of applied compressive force on ERG Duocel aluminium foam and concluded that foam porosity and effective thermal conductivity remain unconstrained with applied force in the range 0 – 2 MPa. The dominant role of the ligament or structural phase of highly porous aluminium for heat conduction in a metal foam-fluid system was investigated in [13] using water, oil and air as the saturating phase. The contributory effect of gas on the effective thermal conductivity of a gas-filled metal foam was found to be negligible while the presence of liquid gains additional significance under conditions that allow liquid circulation in the interstices of the foam cellular space.

Aside from the proposed empirical model in Calmidi & Mahajan [9], comparable research work has also been extended to analytical, empirical and computational approaches to account for the effective thermal conductivity of metal foam-fluid systems. For instance, using the analogy between Ohm's law and Fourier's law – Lemlich [14] proposed an analytical model for the effective thermal conductivity of a metal foam-fluid system as a function of foam porosity and solid thermal conductivity. The Lemlich theory views electrical conduction as occurring only through the Plateau border (struts or ligament in the case of solid foam) and their expression accurately predicts the effective thermal conductivity for air-foam systems but was less successful for water-foam systems. This disparity was attributed to the neglected contribution of nodal resistance at the tetrahedral vertices and the assumption of negligible heat exchange to the saturating fluid in the Lemlich predictive model. This supposition was further substantiated in [15, 16] by proposing different empirical constants to the Lemlich model in [14]. A representative unit cell model was employed in [17, 18] to formulate a simple analytical model for the determination of the effective thermal conductivity for tetrakaidekahedron-shaped aluminium foams, characterised by cuboid node and porosities beyond 90%. Their proposed model was found to be in keeping and consistent with experimental data for high porosity porous metallic structures.

Motivated by the work of Calmidi & Mahajan [9], Boomsma & Poulikakos [19] proposed a three-dimensional (3D) structure-based model for the determination of the effective thermal conductivity of metal foam-fluid systems by assuming a representative cell of porous metal to be a Kelvin tetrakaidekahedron constructed by cylindrical ligaments and cubic nodes. However, Dai et al. [20] identified an inconsistency in [19] and modified their model accordingly by considering the effect of ligament orientation on the effective thermal conductivity thereby increasing the model prediction accuracy. A corrigendum that contained all the significant corrections in the affected predictive model described in [19] was later published by Boomsma & Poulikakos [21]. Working from X-ray computerised tomography (CT) datasets, Ranut et al [22]. used computational fluid dynamics (CFD) to account for the effective thermal conductivity of metal foam-fluid systems with reasonable correlation to experimental scatter for high porosity foams, typically, above 90%. This approach is considered a pore-level technique using X-ray CT for the literal description of the foam geometry and has been used by several researchers [23–27] to account for the effective thermal conductivity and other thermo-fluidic properties of fluid saturated open-cell foams. In a related work considered by Krishnan et al [28]., virtual foam geometries were created by subtracting a unit cell cube from a sphere and using CFD to resolve the heat transfer for a moving fluid across the interstices of the porous matrix. Numerically computed values of the effective thermal conductivity for several replicated matrices compared well with available experimental measurements and semi-empirical models for foam porosities greater than 94%.

A significant number of related articles focusing on the effective thermal conductivity of porous metals are concentrated primarily on high-porosity foams (i.e. $\varepsilon > 0.85$) while only a limited number are associated with low-porosity foams. Typically, experimental measurements adopting the transient plane source for the effective thermal conductivity of AlSi7 foam-fluid systems were reported by Solorzano et al [29]. for porosities between 0.5 and 0.8. Their experimental data showed a dependence of effective thermal conductivity on foam porosity with a significant dependency on the region of foam where the experiment was performed. Abuserwal et al [30]. used the steady-state method to account for the effective thermal conductivity of "bottleneck-shaped" aluminium foams produced by a replication casting technique, characterised by sample porosities between 0.57 to 0.77 and pore sizes between 0.7 and 2.4 mm. The effective thermal conductivity was found to decrease with increasing porosity with no discernible influence on pore size. Furthermore, the impact of pore size variation on the effective thermal conductivity of open-celled copper foams numerically studied in [31], showed a strong dependence on porosity ($0.73 < \varepsilon < 0.97$) for a given pore size distribution in agreement with the experimental work on low-porosity foams reported by Dukhan & Chen [11]. In general, there is little experimental and/or computationally simulated data on the effective thermal conductivity for low-porosity metal foam-fluid systems. This work, therefore, seeks to numerically investigate the

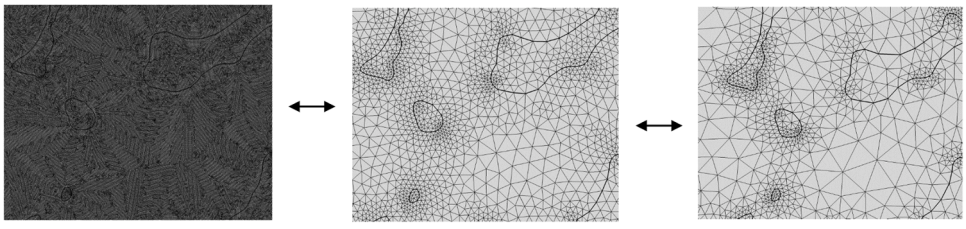

Fig. 1. Left-right, are representation of part of a metal foam-fluid system showing extremely [8–12MCells], normal/optimised [2–3MCells] and coarse [0.7–1.0MCells] linear tetrahedral mesh [LTM] distribution.

contributory effects of fluid and structure on the effective thermal conductivity for low porosity "bottleneck-dominated" metal foam-fluid systems. This work may distinguish itself from other related works through insights into novel 3D advanced image inversion techniques working from high-resolution computer tomography datasets. This work also seeks to provide evidence on the contributory effects of fluid on the overall heat flux in a metal foam-fluid system and empirical constants and indexes for predicting the effective thermal conductivity for low-porosity foams

Research approach

The modelling approach used in this work is categorised into two stages, three-dimensional advanced image inversion and numerical modelling of heat transfer across fluid-saturated porous metallic structures. The porous metallic samples used for this study were produced by a replication casting route as described in [32, 33] but extended in this work to structures categorised by lower porosity ($\varepsilon \leq 0.7$) and smaller cell size ranges ($0.5 \leq D_p \leq 2mm$). In brief, porous metallic structures consisting of 99.5% aluminium (Al) were prepared by infiltrating liquid metal into a mould containing packed beds of near-spherical sodium chloride (NaCl) salts (space holder). The liquid metal was initially heated below the melting point of the salt (800 °C) followed by compaction and preheating (450–600 °C) of the space holder to avoid premature solidification of the melt. Sequestration of the liquid metal into the convergent voids left by the space holders was achieved by an applied infiltration pressure ranging between 0.27 and 0.9 bar before solidification of the melt. The foam-salt material was then machined to obtain the desired shape and size followed by dissolution in a warm ($T \leq 40^oC$) incubation bath for 3 days to proliferate porosity. This structure (as shown by Fig. 1) is termed "bottleneck-shaped" [23, 32–34] due to its near-circular cell size (determined by the salt shape and size) and pore openings (determined by the applied infiltration pressure and contact between neighbouring salts). By varying the cell size and applying differential pressure, several other porous metals of different morphologies and porosities were produced and characterised as shown in Table 1 (to be discussed later).

A Zeiss Xradia XRM-500 3D computerised tomography system was used to acquire high-resolution (26 μm voxel size) 2D datasets for image processing and characterisation. ScanIP module of Synopsys-Simpleware™ (a 3D advanced imaging software) was used to reconstruct a 3D volume of the porous structure from the 2D slices. A workable representative volume of the structure was achieved through cubical reduction of the reconstructed 3D volume until their porosities differ by ±2 per cent. A Boolean inversion of the representative structural domain was done to create the fluid phase and final superimposition of the two phases to create the metal foam-fluid interfaces. A smart masque smoothing approach with 10 iterations was applied to remove unwanted noise in the metal foam-fluid systems and was preferred over recursive Gaussian Smoothing due to the ability of the smart masque approach to preserve sample geometry. The average cell size and pore openings were characterised by measuring the mean value of watershed segmented particles and creating a centreline across the openings of the representative sample, respectively. The +FE module of the Synopsys-Simpleware™ was employed for the discretisation of the metal foam-fluid system into linear tetrahedral cells with optimum cell density ranging between 2 and 3 MCells for all samples studied. The optimum cell density range was achieved by resolving the temperature distribution of a stagnant fluid across the interstices of several meshed samples ranging from coarse ($< 1MCells$) to extremely fine mesh structures ($< 12MCells$) while maintaining a constant cell growth rate of 1.3, as shown by Fig. 1. With a maximum edge length 6x image resolution, the optimum mesh structure (Fig. 1, middle) yielded a metal foam-fluid temperature that is 99.9% convergent with a fine tetrahedral meshed sample thereby minimising simulation time and conserving computational resources, a trade-off between mesh count, convergence and accuracy. Computational fluid dynamics (CFD) modelling and simulations were performed by resolving conductive heat transfer physics on the fluid-foam worked representative geometry in COMSOL Multiphysics. The choice of physical parameters for the metal foam-fluid system was considered because the interstitial fluid and foam domains were assumed motionless (as described in [22, 28, 31, 35]). A temperature difference of 20 °C was maintained between the inlet and outlet fluid boundaries – with the inlet considered to be of higher temperature whilst the lateral faces were considered as thermally insulated walls. Mathematical expressions for the conduction heat transfer and boundary conditions are expressed in Eq. (1) below.

$$\begin{aligned} &\rho C_p u.\nabla T + \nabla.q = Q_{tot}\, where\ \ (Physics) \\ &Inlet\ T = 293.15K\ and\ outet\ T = 273.15K \\ &-n.q = 0\ (Thermallyinsulatedwallsforlateralfaces) \end{aligned} \tag{1}$$

where ρ ~ material density (kg.m^{-3}), C_p~ heat capacity at constant pressure (J.$kg^{-1}.K^{-1}$), u~ velocity component (m.s^{-1}), T~ temperature (K), q~ total net heat rate (W), Q_{tot}~total heat source (W.m^{-3}) and k is the thermal conductivity of the material (W.$m^{-1}.K^{-1}$). This advanced imaging technique coupled with CFD modelling and simulation approaches were repeated for all the porous metal samples produced. Air, water, ethanol vapour and ethanol liquid were considered as the saturating fluid domain while the properties of pure aluminium, copper and nickel were individually selected as the structural domain of the

Table 1
Pore structure-related parameters and predicted effective thermal conductivity of several metal foam-fluid systems.

Samples	Cell size [mm]	Pi [bar]	ε[%]	Dw [mm]	Dp [mm]	$\sigma_{FB} = S_F/V_B$ [m^{-1}]	Al-Air K_{eff}[W.$m^{-1}.K^{-1}$]	Al-H_20 K_{eff}[W.$m^{-1}.K^{-1}$]	Al-Ethanol vapour K_{eff} [W.$m^{-1}.K^{-1}$]	Al-Ethanol liquid K_{eff} [W.$m^{-1}.K^{-1}$]	Ni-Air K_{eff}[W.$m^{-1}.K^{-1}$]	Cu-Air K_{eff}[W.$m^{-1}.K^{-1}$]
A1	0.5–1.0	0.90	65.28	0.178	0.730	7060.6	36.49	37.41	36.48	36.71	9.65	61.29
A2	0.5–1.0	0.33	72.81	0.243	0.721	4934.6	20.90	22.03	20.90	21.17	5.55	35.09
B1	1.0–1.4	0.90	71.34	0.275	1.213	4588.4	27.84	28.76	27.84	28.06	7.37	46.77
B2	1.0–1.4	0.33	72.09	0.321	1.215	4207.0	26.39	27.29	26.39	26.61	6.99	44.32
C1	2.0–2.5	0.90	70.53	0.650	2.230	2590.0	33.46	34.24	33.45	33.65	8.85	56.21
C2	2.0–2.5	0.33	75.21	0.740	2.270	2410.8	27.56	27.56	27.56	27.74	7.29	46.29
C3	2.0–2.5	0.27	78.40	0.900	2.230	2054.4	17.96	18.92	17.95	18.18	4.77	30.15
D1	2.5–3.15	0.90	74.65	0.732	2.774	2244.7	25.82	26.67	25.82	26.03	6.84	43.37
D2	2.5–3.15	0.33	75.08	0.764	2.783	2032.9	21.97	23.00	21.97	22.22	5.83	36.90
C11	Adapted Structures		76.52	0.840	2.290	2214.7	22.76	23.60	22.76	22.96	6.03	38.22
C12			80.88	1.020	2.360	1853.3	15.55	16.44	15.54	15.76	4.13	26.10
C13			86.59	1.151	2.431	1564.4	10.47	11.44	10.47	10.71	2.79	17.57
C14			90.19	1.352	2.484	1062.3	3.14	4.41	3.14	3.48	0.88	5.24
C15			93.03	1.570	2.546	791.3	1.08	2.41	1.07	1.46	0.34	1.75

NB: ε is foam porosity, Ks is solid foam thermal conductivity, Keff is the effective thermal conductivity, Pi is the liquid metal infiltration pressure, Dw is the mean pore opening, Dp is the mean cell/pore size, σ_{FB} is the specific surface defined as the ratio of the foam surface area (S_F) per unit bulk volume (V_B).

representative metal foam-fluid systems during simulation. The effective thermal conductivity of the metal foam-fluid system was obtained by dividing the computed overall conductive heat flux (q, W.m^{-2}) for the system by the computed one-dimensional temperature gradient (Tzz, K.m^{-1}) and multiplying this ratio by a negative of one as described by the experimental work in [9, 11, 29, 30] and predictive approach in [16, 17, 22]. The normalised effective thermal conductivity for all the metal foam-fluid systems was obtained by dividing the CFD predicted effective thermal conductivity by the thermal conductivity of the solid domain under consideration. Lastly, computed values of effective thermal conductivity for low-porosity foams were substituted into empirical correlations developed by Calmidi & Mahajan [9] for the determination of predictive empirical constants. The analytical expression in [9] relates the effective thermal conductivity (k_{eff}) of microcellular structures as a test function of foam porosity (ε), fluid thermal conductivity (k_f), solid thermal conductivity (k_s), empirical constant (A) and index (n) as shown by Eq. (2).

$$\frac{k_{eff}}{k_f} = \varepsilon + A(1-\varepsilon)^n \frac{k_s}{k_f} \tag{2}$$

Analysis of research data

The computational approach considered utilises structure-derived representative volume elements (RVE) characterised by flow pathway or boundary distances smaller in length than the entire domain of a real foam material. This is imperative to minimise the computational power and convergent time needed for resolving the physics across a metal foam-fluid system. Mostafid [36] and De Carvalho et al [37]. considered a 20 – 50 pore diameter size as the appropriate critical thickness for through-flow across tetrakaidekahedron-shaped foam materials. However, related articles [26, 38, 39] on moving fluid across "bottleneck-shaped" structures considered the boundary distance to be 3 – 5x their mean pore diameter – by limiting the porosity difference between a real and CT-derived RVE structure to ±3%. Outside this deviation, there is the possibility that discrepancy between the modelling route and available experimental measurements of the effective thermal conductivity for real foam structures may result from a consequence of representative volume element [37, 40, 41] against topology of the microstructure. A similar computational approach was adopted in this study but extended to inversion and superimposition of fluid and porous matrix domains to form a metal foam-fluid representative volume (known as image-inversion) as described by Fig. 2 below. The technique distinguishes itself from previous reverse engineering approaches of working from X-ray CT datasets [22, 35] and 3D Laguerre-Voronoi Tessellations technique [24, 27] by neglecting surrounding fluid across the 3D metal foam-fluid system. This technique only utilises the fluid occupying the interstices of the foam structure thereby minimizing the required cell density, degrees of freedom, convergence time and computational power required to resolve the physics of a metal foam-fluid system. This approach may well be beneficial in the identification of materials as well as solving for heat conduction across the interstices of structures.

Analysis of the required thickness for these structures was initially made by sectioning smaller RVE from the centre of a 3D CT volume for samples at the two extremities of porosity (i.e. sample A1 and C3 with 0.643 and 0.784 porosities, respectively, as shown in Table 1) and resolving the temperature distribution for the metal foam-fluid RVE samples Fig. 3. presents the temperature profile plots of CFD simulated RVE metal foam-fluid systems at the extremities of porosities – showing the intensity (legend scale [Kelvin]) of increasing/decreasing temperature for both samples. This is an indication that heat is observably transferred in the direction of a temperature gradient. The tendency of a constrictive response is higher for A1 structure (characterised by lower porosity and cell size) when compared to the larger cell size structures (C3). Structure C3 has more volume to accommodate fluid thereby reducing the surface area of its solid domain when compared to structure A1 and this has been shown to contribute to changes in their

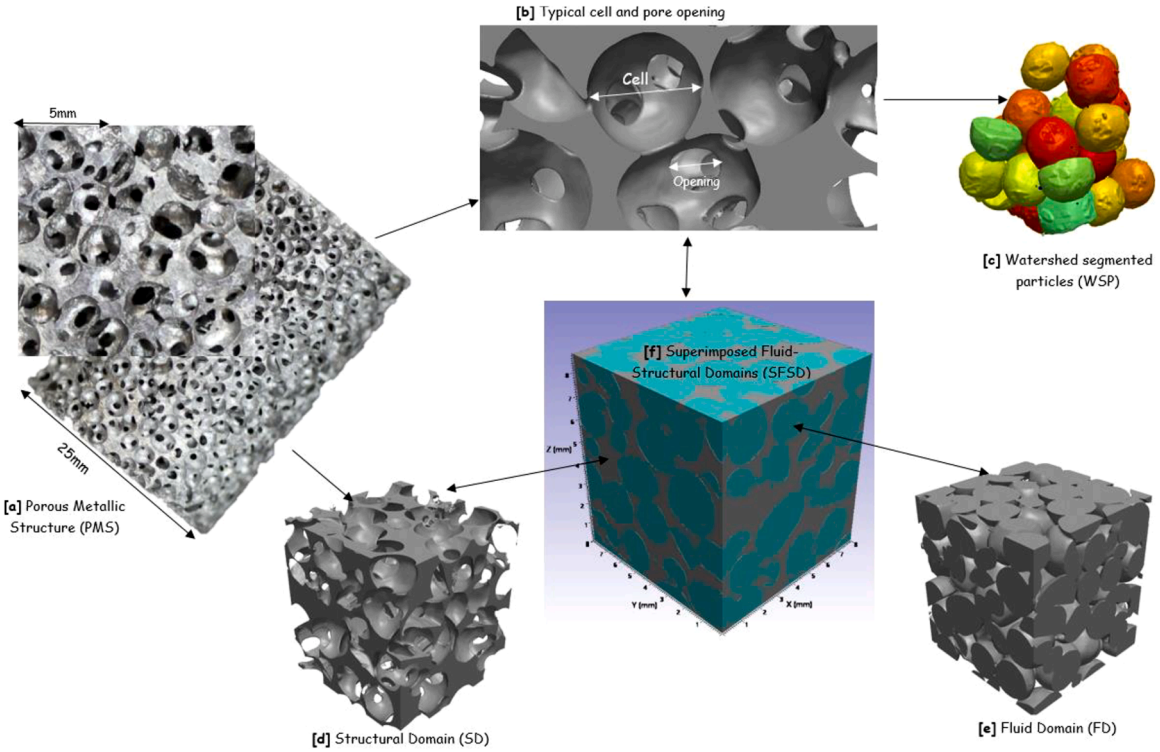

Fig. 2. Three-dimensional (3D) results of advanced image analysis show the following: (a) porous metallic structure [PMS] produced by replication casting route (b) typical cell and pore-openings or "windows" (c) watershed segmented particles [WSP], (d) representative structural domain [SD], (e) representative fluid domain [FD] and (f) representative superimposed fluid-structural domain [SFSD] of the porous matrix characterised by cell size of 2.0–2.5 mm and porosity of 70%.

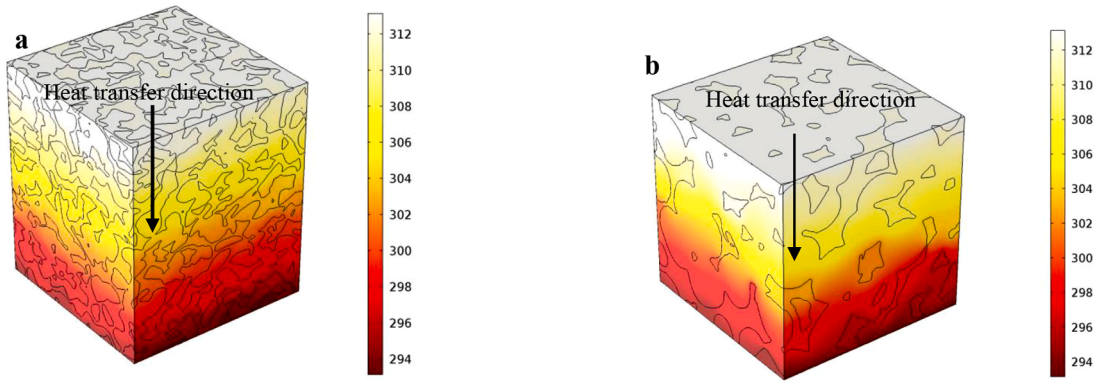

Fig. 3. Three-dimensional temperature [K] distribution plots for A1 [a] and [b] C3 metal foam-fluid system characterised by cell size, applied infiltration pressure and porosity of 0.5–1.0 mm/0.9 bar/0.643 and 2.0–2.5 mm/0.27 bar/0.784 respectively.

effective thermal conductivity, as presented in Table 1 Table 1. shows that the effective thermal conductivity of the more axial distorted and higher pore density (A1) structure is more than twice that of the least distorted material (C3) for all numerically simulated values of the metal foam-fluid systems considered. Even for structures produced with similar cell sizes, the effective thermal conductivity was observably higher for materials produced at higher applied infiltration pressures. This can be attributed to the fact that higher differential pressure enables more penetration of liquid melt into the convergent space provided by the packed space holder (NaCl salts) during casting. The deeper the penetration of liquid melt into the available space the smaller the pore openings and increased surface area available for heat transfer, as shown in Table 1. Conversely reduced applied differential pressure resulted in structures characterised by larger pore openings, lower surface area and decreased effective thermal conductivities.

Table 1 shows that the effective thermal conductivity of the metal foam-fluid systems decreases with a reduction in specific surface area but is accompanied by a slight increase in pore openings and pore size. Similarly, a noticeable change in porosity was observed to be inverse with the effective thermal conductivity of the metal foam-fluid systems. An in-depth understanding of the effects imposed by pore-structure related properties on the effective thermal conductivity of these porous structures was made possible by creating semi-virtual structures which are a facsimile of the original structure using techniques described in [39, 42]. The 3D ScanIP module was used to erode the structural domain of the metal foam-fluid system by removing some pixel element (erosion) thereby influencing the pore structure-related properties of the porous matrix but retaining the overall foam topology. These changes expand the porosity, pore size and pore openings with a consistent decrease in the computed effective thermal conductivity as shown in Table 1 (see sample C11 to C15 obtained from a continuous erosion of sample C1) Fig. 4. presents the temperature profile for computed heat transfer across a real 2D (left) and 3D (middle) sample and 3x eroded sample yielding porosities of 0.703 [C1] and 0.866 [C13] respectively. The effective thermal conductivity of the real sample [C1] was observed to be more than triple for that of the 3x eroded structure [C13] with further decreases seen with increasing sample erosion, as shown in Table 1.

The degree of divergence between the inlet and outlet fluid temperature was observed to exhibit very little or no discernible change on the effective thermal conductivity of the metal foam-fluid systems as shown by Fig. 5b for differential temperatures ranging between 20 and 100 °C. According to the established viewpoints available in the literature [13, 22, 28, 31, 35] - no noticeable change has been observed for both experimental and predictive values of effective thermal conductivity of microcellular structures for/with changes in the fluid differential temperature. Dyga & Witczak [13] described that higher fluid differential temperatures favoured a more or rapid increase in fluid circulation with increasing rapid contacts between fluid particles and pore walls thereby increasing the overall heat flux of the metal foam-fluid system as shown by Fig. 5a. This figure shows that the overall heat flux linearly increases with an increase in the fluid differential temperature with little or no change to their ratio i.e. their effective thermal conductivity. At higher temperatures, the effective thermal conductivity may be more contingent on radiation although conduction remains the simplest heat transfer mechanism and can be achieved only when the fluid in the porous matrix is considered stagnant [9].

To ensure accuracy was maintained, CFD predicted data were substantiated with experimentally measured data available in the literature Fig. 5.c presents the CFD computed (present) and available experimental measurements [9-12, 17, 29, 30] of normalised effective thermal conductivity against foam porosity for the combined real and semi-virtual metal foam-fluid systems. These plots show a linear inverse relationship between the normalised effective thermal conductivity and foam porosity with a reasonable fit of the CFD predicted data to experimental scatter conducted by Dukhan & Chen [11], Solorzano et al [29]. and Abuserwal et al [30].. A probable cause for this concurrence may be attributed to the fact that the experimental measurements were

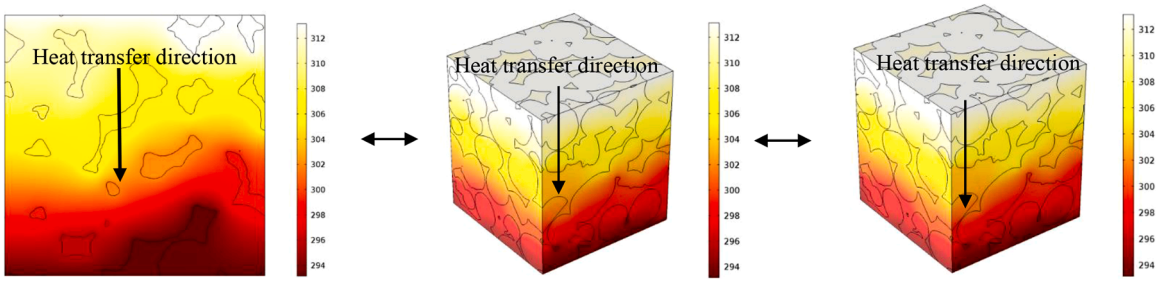

Fig. 4. Left and middle are 2D and 3D temperature [K] distribution across C1 (porosity ~ 0.705) and far-right, is 3x eroded sample of similar foam [C13] characterised by sample porosity of 0.866.

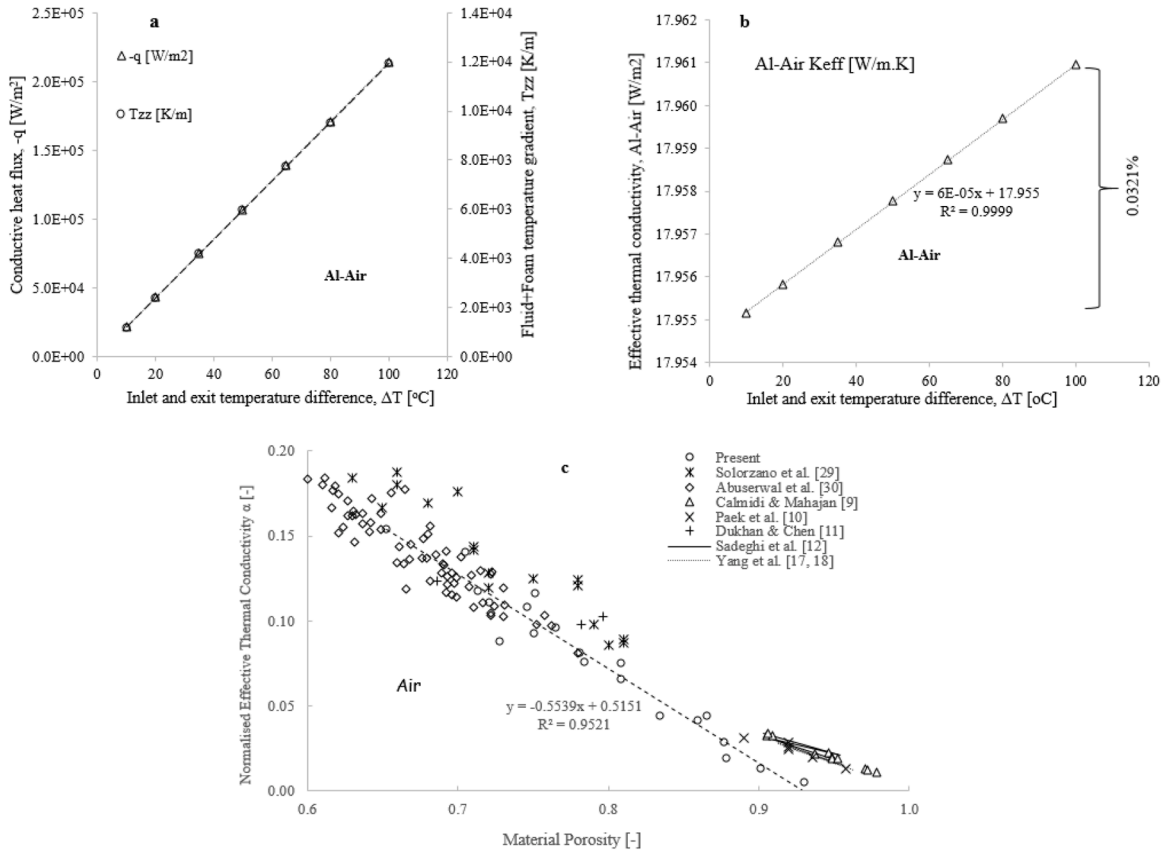

Fig. 5. (a) Plot of the one-dimensional metal foam-fluid conductive heat flux –q [W.m^{-2}] and temperature gradient, Tzz [K.m^{-1}] against inlet and exit temperature difference ΔT [°C], (b) the effect of foam-fluid effective thermal conductivity, Keff [W.m^{-1}.K^{-1}] on the inlet and exit temperature difference and (c) plot of CFD modelled (present) and literature data on normalised effective thermal conductivity against [-] against material porosity [-].

performed on foams manufactured through powder metallurgy [29, 30] and replication casting [11] routes which predominantly result in closed-cell foams with a narrow range of porosities (typically, between 0.5 and 0.78) similar to those considered herein Table 2. highlights this agreement between the CFD predicted and measured data [29, 30] of normalised effective thermal conductivity for some selected metal foam-fluid systems – indicating a more than 94% correlation for all samples presented. It is noteworthy to mention that the creation of semi-virtual structures further extends the linearity to porosity values of 0.93 as shown by Fig. 5c. This figure shows that experimental measurements of the effective thermal conductivity available in [9, 10, 12, 17] were also reportedly performed on highly porous (ε > 0.9) tetrakaidekahedron-shaped materials and provides additional information on continuous decreases in the effective thermal conductivity of metal foam-fluid systems as porosity increases.

Table 2
Validation of numerically simulated data with experimental measurements in [29, 30].

Materials	Cell size& [mm]	ε[%]	Ks[W.m^{-1}.K^{-1}]	Keff[W.m^{-1}.K^{-1}]	α = Keff/Ks [-]	Source
Al6201-Air	0.7–1.0	64.30	205	35.30	0.172	Abuserwal et al [30].
AlSi7-Air	–	65.00	167	27.80	0.166	Solarzano et al [29].
Pure Al-Air	0.5–1.0	65.28	238	36.49	0.153	Present
Al6201-Air	1.0–1.2	72.46	205	22.26	0.109	Abuserwal et al [30].
AlSi7-Air	–	72.00	167	21.40	0.128	Solarzano et al [29].
Pure Al-Air	1.0–1.4	72.09	238	26.39	0.111	Present
Al6201-Air	2.0–2.4	75.78	205	21.22	0.104	Abuserwal et al [30].
AlSi7-Air	–	75.00	167	20.90	0.125	Solarzano et al [29].
Pure Al-Air	2.0–2.5	75.21	238	27.56	0.116	Present

NB: ε is foam porosity, Ks is solid foam thermal conductivity, K_{eff} is effective thermal conductivity and α is the normalised effective thermal conductivity.

Up to now, it has been expedient to describe the effective thermal conductivity of the metal foam-fluid systems as a function of foam porosity Fig. 4. shows that decreasing the foam porosity increases the near-circular pore specific surface, coupled with reduced apertures or pore openings. This continuous increase in ligament thickness of an RVE unit cell results in increased values of effective thermal conductivity (see Table 1). An examination of the contributory effects of the foam or fluid thermal conductivity on the overall effective thermal conductivity would, therefore, be advantageous in understanding the range of influence for this enhancement Fig. 6. presents the contributory effects of varied fluid (a & b) and material (c & d) properties on the effective thermal conductivity and normalised effective thermal conductivity – considering air (k_s = 0.024 $Wm^{-1}.K^{-1}$), water (k_s = 0.6 $Wm^{-1}.K^{-1}$), ethanol vapour (k_s = 0.014 $Wm^{-1}.K^{-1}$) and liquid ethanol (k_s = 0.179 $Wm^{-1}.K^{-1}$) as individual saturating fluids whilst pure aluminium (k_s = 238 $Wm^{-1}.K^{-1}$), nickel (k_s = 106 $Wm^{-1}.K^{-1}$) and copper (k_s = 385 $Wm^{-1}.K^{-1}$) were considered individually as the base solid matrix. By keeping the solid phase properties constant and varying the fluid properties, the difference in the CFD computed data of effective thermal conductivities were observably small when compared to the varied solid-phase properties. Hence, the main mechanism for heat transfer

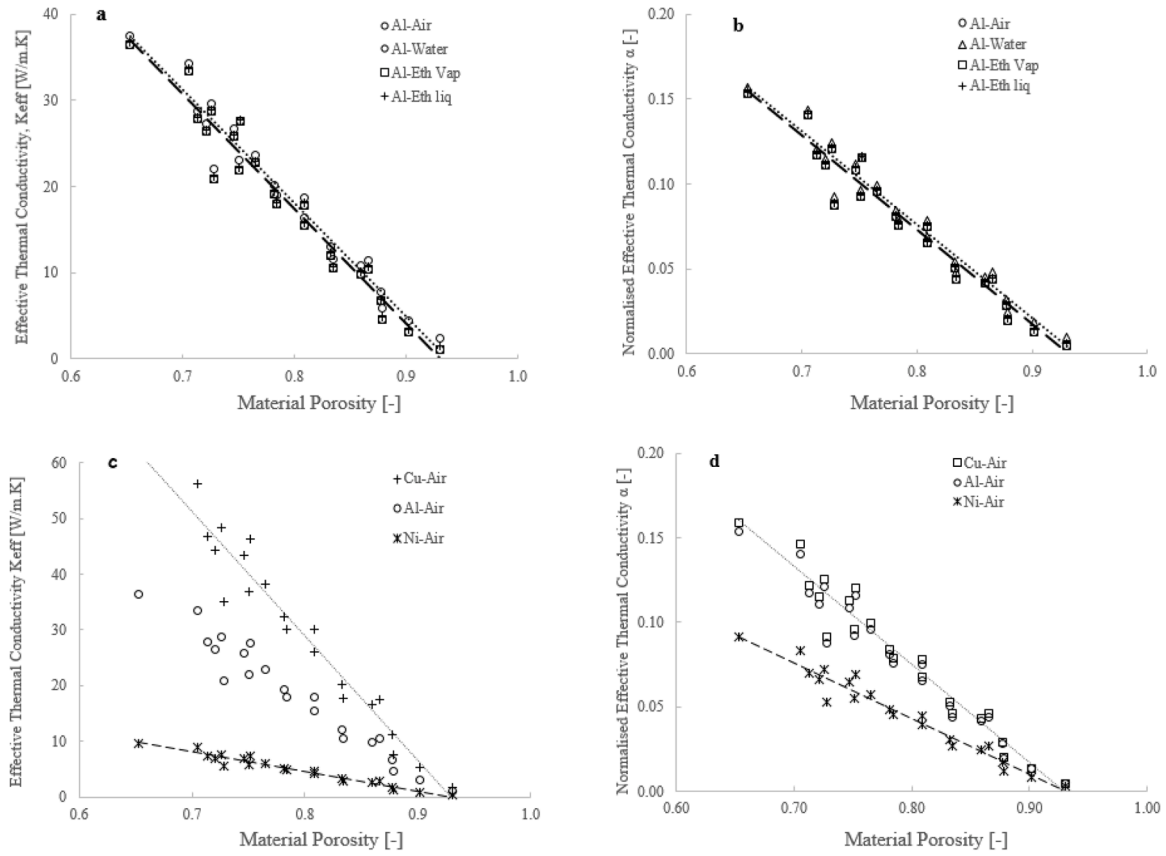

Fig. 6. Plots of effective thermal conductivity, Keff [$W.m^{-1}.K^{-1}$] and normalised effective thermal conductivity, α [-] against material porosity, ε [-] for changes in fluid properties (a & b) and changes in material properties (c & d).

could be described as conduction through the near-circular cell walls (ligaments) of the porous structures. It is, therefore, plausible to say that, a change in the foam porosity would significantly affect the effective thermal conductivity of the metal foam-fluid systems.

Considering the solid phase properties, copper (Cu) has the highest thermal conductivity and heat transfer when compared to pure aluminium (Al) and nickel (Ni) as shown by Fig. 6c. Conversely, the aluminium-ethanol vapour metal foam-fluid system was observed to have the lowest effective thermal conductivity when compared to other applied saturating phases and could be attributed to the very low intrinsic thermal conductivity of the ethanol vapour. The contributory effect imposed by the saturating fluid phase in the metal foam-fluid system was further substantiated by plotting the percentage heat flux of the saturating phases against foam porosity Fig. 7.a shows an exponentially dependant increase of the percentage heat flux on the foam porosity – supporting earlier reported observations in [18, 20, 26, 42, 43 [44]] concerning the dominant role of the water saturating phase over air components. A less than 3 per cent contribution of the saturating gas phases (air and ethanol vapour) to the overall heat transfer mechanism of the metal foam-fluid system was observed when compared to the saturating liquid components (water and ethanol liquid) that more than triple the gas phase contribution. Convection heat transfer was estimated in [28] to contribute up to 4 per cent of the heat transfer across air saturated low-porosity foam. Water has the higher thermal conductivity when compared to other fluid components and would, therefore, be expected to have the most reduced equivalent values of solid-to-fluid conductivity resulting in a significant heat transfer contribution [11] and thereby increasing the overall effective thermal conductivity of a foam-water system [16–19, 24] as shown by Fig. 6a and Fig. 7a Fig. 7.a further supports findings by Barnoon [7] and Alhajaj et al [45]. in terms of heat transfer enhancement using hybrid nanofluids (higher thermal conductivities) in microchannels over pure fluids and could be embodied to fully explain the dominant role of liquid phase heat flux contributions to the overall heat transfer mechanism over gaseous saturating phases.

Since the commercialisation of cellular structures, several related works have been tailored toward high porosity metal foams and sponges typified by porosity (beyond 90 per cent). The effective thermal conductivity of these materials has been shown to strongly depend on foam porosity Eq. (2). is one of several empirical models available in the literature and was reported [9] based on experimental data collected for heat conduction through Al6201-fluid systems. In this work, the best fit to experimental scatter was reported for an empirical index of (n) ~ 0.763 and constant (A): 0.181 and 0.195 for air and water yielding maximum and average absolute errors of 6.9 and 3.7% for air, 7.5 and 3.1% for water respectively. This further illustrates the variability of the effective thermal conductivity on experimentally determined constants with inconsistencies in manufacturing variability and technological operating conditions emblematic in describing this complex microstructure [17, 30, 35]. The "bottleneck-type" microcellular structures considered herein are observed to have lower porosities, therefore, available empirical and structure-derived models for high porosity foams may not necessarily agree with the CFD computed data of effective thermal conductivity for low porosity foams. Hence, it is desirable to obtain an expression or propose empirical constants for the description of the effective thermal conductivity for these structures. From Eq. (2), plots of reduced effective thermal conductivity $ln\left(\frac{k_{eff}}{k_f} - \varepsilon.\frac{k_f}{k_s}\right)$ against ln $(1-\varepsilon)$ in Fig. 7b were observed to show a direct linear relationship but with differences in calculated values of their empirical constants – bringing robust support to the supposition that generalised values for these constants would be ambiguous to fully describe heat transfer

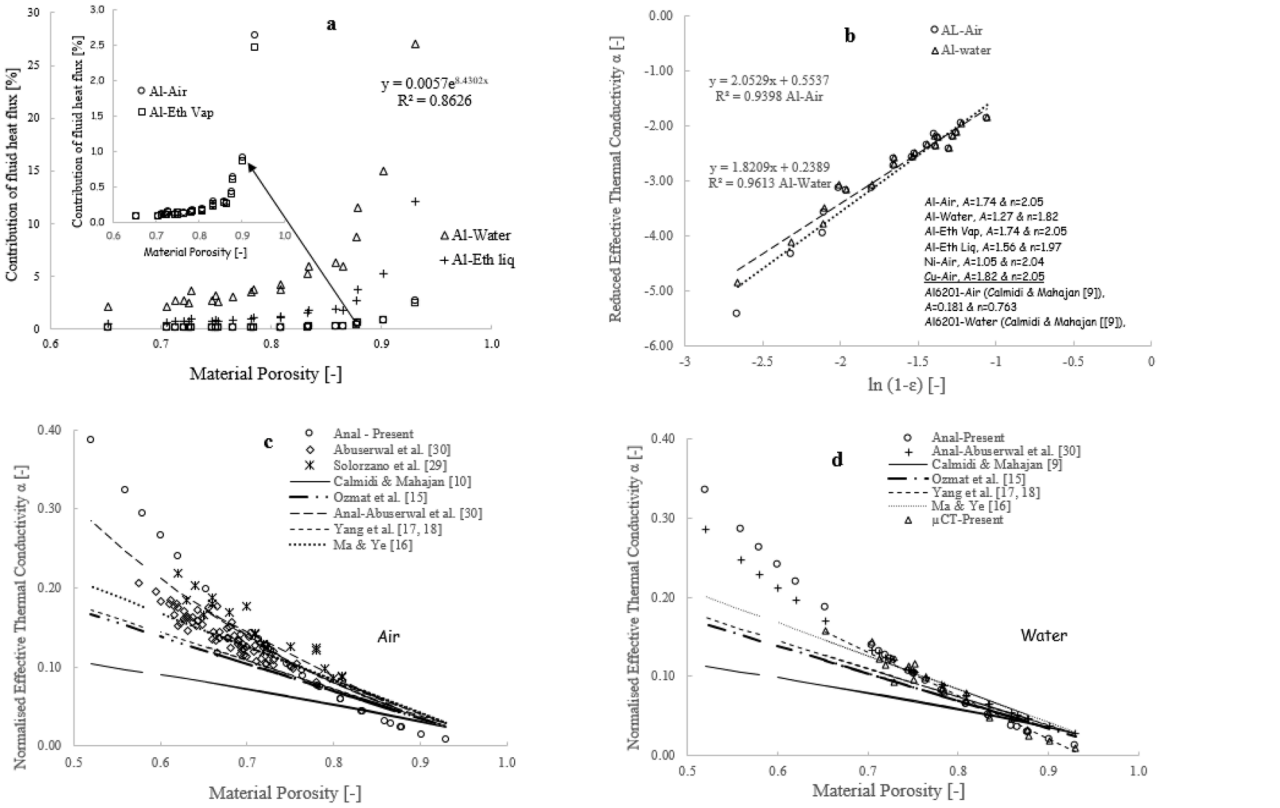

Fig. 7. Plots of (a) contributory effect of fluid heat flux on metal foam-fluid system against material porosity, (b) normalised effective thermal conductivity against material porosity for the determination of empirical constant and index in Calmidi & Mahajan [9] proposed model (c) validation using proposed empirical constant and index against several other analytical models for air and (d) water as saturating fluid.

mechanisms across all metal foam-fluid systems Fig. 7.c and Fig. 7d show that the application of the empirical constants in [9] and other empirical models for high porosity foams underestimate the CFD computed values of effective thermal conductivity studied. The closest fit for CT-derived data is the analytical model described in [30] for low porosity foams similar to the range of porosities considered herein. However, minor differences between calculated values of effective thermal conductivity using the model described in [28] and the application of the calculated values of empirical constants in this work were observed for porosities below 60%. Hence, an insight into CFD computation for much lower porosities, typically, between 50 and 60% may reveal more information and/or possible adjustment to the empirical constants. It is, therefore, presumed pertinent to limit the possible application of the calculated values of empirical constants for heat conduction in "bottleneck-type" structures for porosities between 60 and 80 per cent.

It is also noteworthy to appreciate that available supported experimental measurements for this modelling route were reported for heat transfer mechanism on air- and water-saturated highly-porous metallic structures, mostly, for tetrakaidekahedron-shaped foams. Supportable data on heat transfer mechanisms across low porosity foams in [11, 29, 31] were conducted using only air as the saturating fluid phase and would, therefore, require more experimental measurements for varied fluid properties to fully support this modelling approach for "bottleneck-type" structures. More so, several reports on heat transfer in porous metals showed that no noticeable changes in the effective thermal conductivity of the metal foam-fluid system were observed for variable cell sizes. They draw their conclusions with a higher degree of emphasis on the effect imposed by sample porosity on effective thermal conductivity of the metal foam-fluid system and less emphasis on other pore-structure related properties, most especially, their specific surfaces Table 1. shows that the creation of semi-virtual structures stretches the porosity and specific surface of the samples to a linear inverse relationship and direct quadratic relationship with the effective thermal conductivity of the metal foam-fluid system, respectively. Keeping these two properties constant would be difficult to achieve considering the current processing routes in the manufacturing of foam samples but could aid in fully exploring the possible changes imposed by varied cell sizes and cell openings on the effective thermal conductivity for these structures. Hence, a consideration of heat transfer mechanisms across virtual macroporous structures using sphere packing models in [46] could be useful in exploring the possible changes associated with varying widely the cell size and cell openings of "bottleneck-type" structures on their effective thermal conductivity.

Summary

The modelling route considered reliably predicts the effective thermal conductivity of "bottleneck-type" metallic structures manufactured by a replication casting technique. Modelling results were observed to fit well into available experimental data of effective thermal conductivity for a similar range of porosities. The inversion and superimposition of the fluid and solid domains of the 3D RVE CT samples provide useful information utilising reduced meshed volumes and convergence times for resolving the selected physics and boundary conditions imposed on metal foam-fluid systems. The creation of 3D semi-virtual structures that bear resemblance to real-foam structures further stretches porosities to near-unity and enables an understanding of how changing pore-structure related properties of cellular materials can modulate the effective thermal conductivity for several metal foam-fluid systems. This technique also quantifies the contributory effects of saturating fluid phases on the overall heat flux of metal foam-fluid systems and empirical constants were obtained which could assist manufacturers in the design of load-bearing porous metallic components for applications specific to

conduction heat transfer.

Declaration of Competing Interest

The authors declare that they have no known competing financial interests or personal relationships that could have appeared to influence the work reported in this paper.

Acknowledgement

AJ would like to acknowledge the support of Andrew R. Kennedy, Rory Screaton, The University of Nottingham, (Nottingham, United Kingdom), Federal University of Technology (Minna, Nigeria), Petroleum Technology Development Fund (Abuja, Nigeria), Synopsys-Simpleware Ltd (California, USA) and Bowers & Wilkins Group (West Sussex, United Kingdom) for the provision of technical support, foams and licenses.

References

[1] D. Brough, H. Jouhara, The aluminium industry: a review on state-of-the-art technologies, environmental impacts and possibilities for waste heat recovery, Int. J. Thermofluids 1-2 (2020), 100007, https://doi.org/10.1016/j.ijft.2019.100007.
[2] A.J. Otaru, M. Abdulkadir, M.R. Corfield, A. Kenfack, N. Tanko, Computational evaluation of effective transport properties of differential microcellular structures, AIChE J (2020), https://doi.org/10.1002/aic.16928 e16928.
[3] P.Berke Ghazi, K. Ehab Moustafa Kamel, B. Sonon, C. Tiago, T.J. Massarat, Multiscale computational modelling of closed-cell metallic foams with detailed microstructural morphological control, Int. J. Eng. Sci. 143 (2019) 92–114, https://doi.org/10.1016/j.ijengsci.2019.06.012.
[4] N. Dukhan, P. Patel, Equivalent particle diameter and length scale for pressure drop in porous metals, Exp. Therm. Fluid Sci. 32 (2008) 1059–1067, https://doi.org/10.1016/j.expthermflusci.2007.12.001.
[5] T. Adibi, A. Sojoudi, S.C. Saha, Modelling of thermal performance of a commercial alkaline electrolyzer supplied with various electrical currents, Int. J. Thermofluids 13 (2022), 100126, https://doi.org/10.1016/j.ijft.2021.100126.
[6] A.J. Otaru, O.E. Odumu, Z. Manko, A.G. Isah, R.O. Isa, M.R. Corfield, The impact of microcellular structures on the sound absorption spectra for automotive exhaust performance spectra, Appl. Acoust. 187 (2022), 108508, https://doi.org/10.1016/j.apacoust.2021.108508.
[7] P. Barnoon, Numerical assessment of heat transfer and mixing quality of a hybrid nanofluid in a microchannel equipped with a dual mixer, Int. J. Thermofluids 12 (2021), 100111, https://doi.org/10.1016/j.ijft.2021.100111.
[8] R. Dyga, S. Witczak, Investigation of effective thermal conductivity of aluminium foams, Procedia Eng. 42 (2012) 1088–1099, https://doi.org/10.1016/j.proeng.2012.07.500.
[9] V.V. Calmidi, R.L. Mahajan, The effective thermal conductivity of high porosity fibrous metal foams, ASME J. Heat Transf. 121 (1999) 466–471, https://doi.org/10.1115/1.2826001.
[10] J.W. Paek, B.H. Kang, S.Y. Kim, J.M. Hyun, Effective thermal conductivity and permeability of aluminium foam materials, Int. J. Thermophysics 21 (2) (2000) 453–464, https://doi.org/10.1023/A:1006643815323. Vol.
[11] N. Dukhan, K.C. Chen, Heat transfer measurements in metal foam subjected to constant heat flux, Exp. Therm. Fluid Sci. 32 (2007) 624–631, https://doi.org/10.1016/j.expthermflusci.2007.08.004.
[12] E. Sadeghi, S. Hsieh, M. Bahrami, Thermal conductivity and contact resistance of metal foams, J. Phys. D: Appl. Phys. 44 (2011) (2011), 125406, https://doi.org/10.1088/0022-3727/44/12/125406.
[13] R. Dyga, S. Witczak, Investigation of effective thermal conductivity of aluminium foams, Procedia Eng. 42 (2012) (2012) 1088–1099, https://doi.org/10.1016/j.proeng.2012.07.500.
[14] R. Lemlich, A theory for the limiting conductivity of polyhedral foam at low density, J. Colloid Interface Sci. 64 (1978) 107–110, https://doi.org/10.1016/0021-9797(78)90339-9.
[15] B. Ozmat, B. Leyda, B. Benson, Thermal applications of open-cell metal foams, Mater. Manuf. Process. 19 (5) (2004) 839–862, https://doi.org/10.1081/AMP-200030568.
[16] M. Ma, H. Ye, An image analysis method to obtain the effective thermal conductivity conductivity of metallic foams via a reduced concept of shape factor, Appl. Therm. Eng. 73 (2014) 1279–1284, https://doi.org/10.1016/j.applthermaleng.2014.08.064, 2014.
[17] X.H. Yang, J.J. Kuang, T.J. Lu, F.S. Han, T. Kim, A Simplistic analytical unit cell-based model for the effective thermal conductivity of high porosity open-cell metal foams, J. Phys. D 46 (2013), 255302, https://doi.org/10.1088/0022-3727/46/25/255302.
[18] H. Yang, J.X. Bai, Y.B. Yan, J.J. Kuang, T.J. Lu, T. Kim, An analytical unit cell model for the effective thermal conductivity of high porosity open-cell metal foams, Transp. Porous Med. 102 (2014) (2014) 403–426, https://doi.org/10.1007/s11242-014-0281-z.
[19] K. Boomsma, D. Poulikakos, On the effective thermal conductivity of a three-dimensional structured fluid-saturated metal foam, Int. J. Heat Mass Transf. 44 (2001) 827–836, https://doi.org/10.1016/S0017-9310(00)00123-X.
[20] Z. Dai, K. Nawaz, Y.G. Park, J. Bock, A.M. Jacobi, Correcting and extending the Boomsma–Poulikakos effective thermal conductivity model for three-dimensional fluid-saturated metal foams, Int. Commun. Heat Mass Transf. 37 (2010) 575–580, https://doi.org/10.1016/j.icheatmasstransfer.2010.01.015.
[21] K. Boomsma, D. Poulikakos, Corrigendum for the paper, K. Boomsma, D. Poulikakos, On the effective thermal conductivity of a three-dimensionally structured fluid-saturated metal foam, Int. J. Heat Mass Transf. 44 (2001) 827–836, https://doi.org/10.1016/S0017-9310(00)00123-X, 54 (2011) 746-748.
[22] P. Ranut, E. Nobile, L. Mancini, High-resolution microtomography-based CFD simulation of flow and heat transfer in aluminium metal foams, Appl. Therm. Eng. 69 (2) (2013) 230–240, https://doi.org/10.1016/j.applthermaleng.2013.11.056.
[23] A.J. Otaru, H.P. Morvan, A.R. Kennedy, Measurement and simulation of pressure drop across replicated microcellular aluminium in the Darcy-Forchheimer regime, Acta Mater. 149 (2018) 265–275, https://doi.org/10.1016/j.actamat.2018.02.051.
[24] J. Skibinski, K. Cwieka, S.H. Ibrahim, T. Wejrzanowski, Influence of pore size variation on thermal conductivity of open-porous foams, Materials (Basel) 12 (2019) 1–10, https://doi.org/10.3390/ma12122017, 2019.
[25] M. Zafari, M. Panjepour, M.D. Emami, M. Meratian, Microtomography-based numerical simulation of fluid flow and heat transfer in open-cell metal foams, Appl. Therm. Eng. 80 (2015) 347–354, https://doi.org/10.1016/j.applthermaleng.2015.01.045.
[26] X. Fan, X. Ou, F. Xing, G.A. Turley, P. Denissenko, M.A. Williams, N. Betail, C. Pham, A.A. Lapkin, Microtomography-based numerical simulations of heat transfer and fluid flow through β-sic open-cell foams for catalysis, Catal. Today 278 (2) (2016) 350–360, https://doi.org/10.1016/j.cattod.2015.12.012, 2016.
[27] Z. Nei, Y. Lin, Q. Tong, Numerical investigation of pressure drop and heat transfer through open cell foams with 3D Laguerre-Voronoi model, Int. J. Heat Mass Transf. 113 (2017) 819–839, https://doi.org/10.1016/j.ijheatmasstransfer.2017.05.119.
[28] S. Krishnan, J.Y. Murthy, S.V. Garimella, Direct simulation of transport in open-cell metal foam, ASME J. Heat Transf. 128 (2006) 793–799, https://doi.org/10.1115/1.2227038.
[29] E. Solorzano, J.A. Reglero, M.A. Rodriguez-Perez, D. Lehmbus, M. Wichman, J. A. de Saja, An experimental study on the thermal conductivity of aluminium foams by using the transient plane source method, Int. J. Heat Mass Transf. 51 (2008) 6259–6267, https://doi.org/10.1016/j.ijheatmasstransfer.2007.11.062, 2008.
[30] A.F. Abuserwal, E.M.E. Luna, R. Goodall, R., R.Woolley, The effective thermal conductivity of open cell replicated aluminium metal sponges, Int. J. Heat Mass Transf., Vol. 108(B) (2017) 1439–1448. 10.1016/j.ijheatmasstransfer.2017.01.023.
[31] J. Skibinski, K. Cwieka, S.H. Ibrahim, T. Wejrzanowski, Influence of pore size variation on thermal conductivity of open-porous foams, Materials (Basel) 12 (2019) 1–10, https://doi.org/10.3390/ma12122017, 2018.
[32] A.J. Otaru, H.P. Morvan, A.R. Kennedy, Airflow measurement across negatively-infiltration processed porous aluminium structures, Am. Inst. Chem. Eng. AIChE J. 65 (2019) 1355–1364, https://doi.org/10.1002/aic.16523. Vol.
[33] A.R. Kennedy, Porous metals and metal foams made from powders, In (Ed.), Powder Metall. (2012), https://doi.org/10.5772/33060. IntechOpen.
[34] A.J. Otaru, M.B. Samuel, Pore-level CFD investigation of velocity and pressure dispositions in microcellular structure, Mater. Res. Express 8 (2021), 046516, https://doi.org/10.1088/2053-1591/abf3e2.
[35] P. Ranut, E. Nobile, On the effective thermal conductivity of metal foams, J. Phys.: Conf. Series 547 (2014), 012021, https://doi.org/10.1088/1742-6596/547/1/012021. IOP Publishing.
[36] A.M. Mostafid, Entrance and exit effect on flow through metallic foams. Department of Mechanical and Industrial Engineering, Concordia University, Quebec, Canada, 2007 https://www.academia.edu/7485936/Entrance_and_Exit_Effects_on_Flow_through_Metallic_Foams.
[37] T.P. De Carvalho, H.P. Morvan, D. Hargreaves, H. Oun., A.R. Kennedy, Pore-scale numerical investigation of pressure drop behaviour across open-cell metal foams, Transp. Porous Med, 117(2) (2017) 311–336 10.1007/s11242-017-0835-y.
[38] T.G. Zielinski, On the representativeness of the representative cells for the microstructural-based predictions of sound absorption in fibrous and porous media. European Acoustics Association. EuroNoise 2015 https://www.semanticscholar.org/paper/On-representativeness-of-the-representative-cells-Zieli%C5%84ski/b4d2cd7eddb03156052836f358f10b14e76b6d4f.
[39] A.J. Otaru, The permeability of replicated microcellular structures in the Darcy regime, Am. Inst. Chem. Eng. AIChE J. 66 (5) (2020) e1691510.1002/aic.16915.
[40] J. Petrasch, P. Wyss, A. Steinfeld, Tomography-based monte carlo determination of radiative properties of reticulated porous ceramics, J. Quant. Spectrosc. Radiat. Transf. 105 (2007) 180–197, https://doi.org/10.1016/j.jqsrt.2006.11.002, 2007.
[41] K.K. Bodla, J.Y. Murthy, S.V. Garimella, Microtomography-based simulation of transport through open-cell metal foams, Numer. Heat Transf., Part A: Appl. 58 (7) (2010) 527–544, https://doi.org/10.1080/10407782.2010.511987.
[42] A.J. Otaru, Enhancing the sound absorption performance of porous metals using tomography images, Appl. Acoust. 143 (2019) 183–189, https://doi.org/10.1016/j.apacoust.2018.09.007, 2019.
[43] M.S. Phanikumar, R.L. Mahajan, Non-darcy natural convection in high porosity metal foams, Int. J. Heat Mass Transf. 45 (2002) 3781–3793, https://doi.org/10.1016/S0017-9310(02)00089-3.

[44] V.V.Calmidi Bhattacharya, R.L. Mahajan, Thermophysical properties of high porosity metal foams, Int. J. Heat Mass Transf. 45 (2002) 1017–1031, https://doi.org/10.1016/S0017-9310(01)00220-4.
[45] Z. Alhajaj, A.M. Bayomy, M. Ziad Saghir, M.M. Rahman, Flow of nanofluid and hybrid fluid in porous channels: experimental and numerical approach, Int. J. Thermofluids 1-2 (2020), 100016, https://doi.org/10.1016/j.ijft.2020.100016, 2020.
[46] A.J. Otaru, A.R. Kennedy, The permeability of virtual macroporous structures generated by sphere-packing models: comparison with analytical models, Scr. Mater. 124 (2016) 30–33, https://doi.org/10.1016/j.scriptamat.2016.06.037.